coatings

MDPI

Article

Polyethylene Glycol (PEG) Modified Porous $Ca_5(PO_4)_2SiO_4$ Bioceramics: Structural, Morphologic and Bioactivity Analysis

Pawan Kumar [1,*], Meenu Saini [1,*], Vinod Kumar [2], Brijnandan S. Dehiya [1], Anil Sindhu [3], H. Fouad [4,5,*], Naushad Ahmad [6], Amer Mahmood [7] and Mohamed Hashem [8]

1 Department of Materials Science and Nanotechnology, Deenbandhu Chhotu Ram University of Science and Technology, Murthal 131039, India; drbrijdehiya.msn@dcrustm.org
2 Department of Biotechnology, Deenbandhu Chhotu Ram University of Science and Technology, Murthal 131039, India; indoravinod2@gmail.com
3 Department of Bio and Nanotechnology, Guru Jambheshwar University of Science and Technology, Hisar 125001, India; sindhu.anil@gmail.com
4 Applied Medical Science Department, Community College, King Saud University, P.O. Box 10219, Riyadh 11433, Saudi Arabia
5 Biomedical Engineering Department, Faculty of Engineering, Helwan University, P.O. Box, Helwan 11792, Egypt
6 Chemistry Department, College of Science King Saud University, Riyadh 11451, Saudi Arabia; exactlykot@gmail.com
7 Stem Cell Unit, Department of Anatomy, College of Medicine, King Saud University, Riyadh 11461, Saudi Arabia; amer_dk@yahoo.com
8 Dental Health Department, College of Applied Medical Sciences, King Saud University, P.O Box 10219, Riyadh 11433, Saudi Arabia; mihashem@ksu.edu.sa
* Correspondence: pawankamiya@yahoo.in (P.K.); meenu.rschmsn@dcrustm.org (M.S.); menhfef@ksu.edu.sa (H.F.)

Received: 10 March 2020; Accepted: 29 May 2020; Published: 31 May 2020

Abstract: Bioceramics are class of biomaterials that are specially developed for application in tissue engineering and regenerative medicines. Sol-gel method used for producing bioactive and reactive bioceramic materials more than those synthesized by traditional methods. In the present research study, the effect of polyethylene glycol (PEG) on $Ca_5(PO_4)_2SiO_4$ (CPS) bioceramics was investigated. The addition of 5% and 10% PEG significantly affected the porosity and bioactivity of sol-gel derived $Ca_5(PO_4)_2SiO_4$. The morphology and physicochemical properties of pure and modified materials were evaluated using scanning electron microscopy (SEM), X-ray powder diffraction (XRD), transmission electron microscopy (TEM) and Fourier-transform infrared spectroscopy (FTIR), respectively. The effect of PEG on the surface area and porosity of $Ca_5(PO_4)_2SiO_4$ was measured by Brunauer–Emmett–Teller (BET). The results obtained from XRD and FTIR studies confirmed the interactions between PEG and CPS. Due to the high concentration of PEG, the CPS-3 sample showed the largest-sized particle with an average of 200.53 µm. The porous structure of CPS-2 and CPS-3 revealed that they have a better ability to generate an appetite layer on the surface of the sample when immersed in simulated body fluid (SBF) for seven days. The generation of appetite layer showed the bioactive nature of CPS which makes it a suitable material for hard tissue engineering applications. The results have shown that the PEG-modified porous CPS could be a more effective material for drug delivery, implant coatings and other tissue engineering applications. The aim of this research work is to fabricate SBF treated and porous polyethylene glycol-modified $Ca_5(PO_4)_2SiO_4$ material. SBF treatment and porosity of material can provide a very useful target for bioactivity and drug delivery applications in the future.

Keywords: calcium phosphate silicate; PEG; bioceramics; sol-gel preparation; hard tissue engineering

1. Introduction

$Ca_5(PO_4)_2SiO_4$ bio-ceramic is a fully loaded compound consisting of Ca, P and Si elements [1]. The calcium–phosphate–silicate (CPS) ceramics are considered as biocompatible materials which is exclusively utilized as implantable materials for bone defects repairing [2]. Silicon-based bioceramics permit to form a functional silanol group with Si–O–H connectivity on the material surface [3]. The silanol group induces the formation of bone-like apatite by attracting Ca^{2+} and PO_4^{3-} through an ion-exchange process in an artificial solution similar to blood plasma [4,5]. This apatite is broadly utilized biomaterial to repair and reconstruct hard tissue defects [6,7]. Thus, researches on silicon-containing bioceramics have received a considerable attention from the biomaterials scientists as such biomaterials are considered as bone substitute materials [8,9]. However, various drawbacks such as less mechanism properties, low chemical stability and reduced bioactivity, the clinical applications of CPS bioceramics are limited [10,11]. It was researched that for a reliable bone fixation, the porosity of implant material should be over 70% so that the body fluids can penetrate easily for the better bone growth [12,13]. In order to get a bioactive and porous material, sol-gel derived polyethylene glycol-modified CPS was prepared in which polyethylene glycol (PEG) was used to modify the phase of $Ca_5(PO_4)_2SiO_4$ via crosslinking of PEG diacrylate chain with PO_4^{3-} and Ca^{2+} probably by the OH^- exchange reactions [14,15]. PEG has been widely accepted as a phase change material, which can be altered through its congruent melting behavior and low vapor pressure [16]. Low molecular weight polyethylene glycol (PEG) is a highly non-immunogenic, non-toxic, biocompatible and biodegradable polymer [17,18]. It possesses a straight poly-ether diol chain that has hydroxyl groups and also shows covalent binding with proteins, phospholipids, functional groups, fluorescent probes, etc [19]. PEG will be a promising agent that may enhance the biocompatibility of $Ca_5(PO_4)_2SiO_4$ by generating porosity in the material. The use of larger PEG chains resulted in more agglomerated hollow particles [20]. Sol-gel process is a flexible and favorable method due to its low-temperature, high purity, easy doping and cost effective approach to prepare various nanocomposites and other nanobiomaterials [21,22]. The reaction time may affect the particle size and stability in the sol-gel process [23]. During the reaction monomers converted into colloidal solution (sol) and then into gel or integrated network of discrete particles [24,25]. Due to bioactive properties, the silica-based glass networks are prepared in various shapes, sizes and hence applied for variety of biomedical applications [26]. Sol-gel synthesized bioceramics are highly biocompatible with controlled degradation rate and effortlessly metabolized in the body [27,28].

In the current research work, we synthesized a pure phase of $Ca_5(PO_4)_2SiO_4$ and PEG-modified porous $Ca_5(PO_4)_2SiO_4$ bioceramic materials through the sol-gel method and investigated various properties. The highly bioactive and porous PEG-modified CPS can be utilized for tissue engineering and drug delivery.

2. Materials and Methods

2.1. Synthesis of Porous Calcium Phosphate Silicate

Sol-gel synthesis was convenient because it permits direct fabrication of bioceramics with different configurations. The synthesis of PEG-modified $Ca_5(PO_4)_2SiO_4$ was carried out as follows: 12.17 mL tetraethyl orthosilicate (TEOS, ≥98% Sigma Aldrich, Saint Louis, MO, USA), 150 mL ethanol, 0.80 g P_2O_5 (≥99.9% Sigma Aldrich) and 6.68 g $Ca(NO_3)_2{\cdot}4H_2O$ (≥99.9% Sigma Aldrich) was mixed stepwise to get 680 mL homogenous mixture. To make composite, 5% and 10% *w/v* of PEG 400 were dispersed in 100 mL distilled water and mix with the above mentioned homogenous mixture. In acidic conditions, TEOS completely hydrolyzed and obtained $Si(OH)_4$ which slow down the condensation rate [22].

Add ammonia (25%) solution to make pH 11 of the mixture which boosts the rate of the gelation process, ideal for the formation of smaller aggregates. TEOS works as a principal network forming agent during gelation. The change in synthesis conditions or parameters such as pH, temperature and additives affect the silica-based glass networks which produce various shapes, sizes and formats products [26]. The different steps used for the synthesis of PEG-modified $Ca_5(PO_4)_2SiO_4$ are shown through the schematic diagram, see Figure 1. Naming of the samples was done on the basis of concentration variation of additive, i.e., PEG in $Ca_5(PO_4)_2SiO_4$; for pure $Ca_5(PO_4)_2SiO_4$ without PEG was assigned to CPS-1. Similarly, for PEG 5% ND 10% by weight in $Ca_5(PO_4)_2SiO_4$ was assigned CPS-2 and CPS-3, respectively. Further, these three samples were used for different characterization.

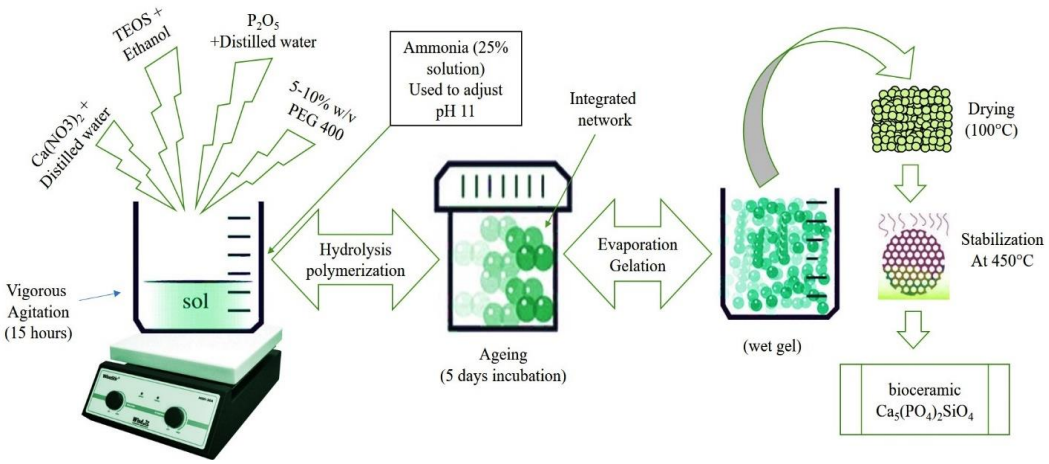

Figure 1. Synthesis of porous calcium phosphate silicate.

2.2. Characterizations of Porous Calcium Phosphate Silicate

The phase identification of the synthesized materials was investigated using XRD (Rigaku Ultima IV, Tokyo, Japan). The measurement was taken at 45 kV voltage and 40 mA anodic current. XRD patterns were acquired at a diffraction angle from 15° to 60°. The compositional information of the prepared samples was investigated by FTIR (Perkin Elmer Frontier FTIR, MA, USA). First, the obtained powder was mixed with KBr in an appropriate ratio and then after applying pressure. The mixture was converted into pellets. For investigations of obtained spectra, the background spectra were calibrated with KBr. The morphology and elemental composition of the samples was examined using SEM (JEOL, JSM 6100, Akishima, Tokyo, Japan) and by energy dispersive spectroscopy (EDS) attached with same, respectively. On sputter was then to sputter coat the samples with a palladium layer. After 30 nm palladium coating, observations were done at an accelerating voltage of 20 kV and 10 Pa. The powerful size of the pore was figured as the mean distances across of sample pores. The nanoparticles synthesis confirmed through TEM (TECNAI 200 kV, Hillsboro, OR, USA) at SAIF in AIIMS, New Delhi. To provide contrast under magnification, nanoparticles were suspended in water (1 mg/mL), placed on copper grids of 0.037-mm size and then stained with a 2 g/100 mL uranyl acetate aqueous stain. Before viewing under 50,000 to 120,000 times magnification, surplus liquid on Mesh was wiped off with filter study and the grid was allowed to air dry. Observations were performed at 80 kV. Brunauer–Emmett–Teller (BET) (BELSORP mini II, Osaka, Japan) technique was used to measure the porosity and surface area of the prepared materials. Tris-HCl-buffered synthetic body fluid (SBF) was used to check bioactivity of the sample after 7 days at 37 °C in an incubator. The thermal stability of the prepared material was evaluated by the thermogravimetric analysis (TGA; Perkin Elmer STA 6000, Waltham, MA, USA) operated under nitrogen flow in the temperature range from 50 to 800 °C at 10 °C/min. Using TGA, by inducing heat to the sample, the chemical reactions and physical changes due to dehydration, decomposition and oxidation can be evaluated.

3. Results and Discussion

3.1. Physiochemical Analysis of Calcium Phosphate Silicate Materials

The sol-gel derived white powdered samples of CPS and PEG-modified CPS were heated at 450 °C to get phase or structural transformation. In the XRD spectra, the distinct peaks of the pure phase of CPS-1 were identified and matched with the standard database card number 00-901-1950 and PDF 40-0393 [29].

The XRD patterns of the PEG-modified CPS bioceramics showed modification in peaks [30]. The addition of 5% and 10% PEG in CPS make some changes in the sample, generate and demolish several phases or peaks in CPS-2 and CPS-3 (Figure 2A). The heat treatment (450 °C) to CPS-2 (5% PEG) and CPS-3 (10% PEG) removed the precursor residues of PEG, limiting the densification of material [31]. During the heat treatment, PEG started to decompose within a temperature range of around 250–300 °C; this can completely remove PEG from the sample [32,33]. The removal/degradation of PEG may generate a porous structure due to structural rearrangement by various chemical reactions, based on several treatment temperature and duration. The sintered sample of CPS-2 (5% PEG) and CPS-3 (10% PEG) also confirmed the presence of wollastonite [PDF 50–0905].

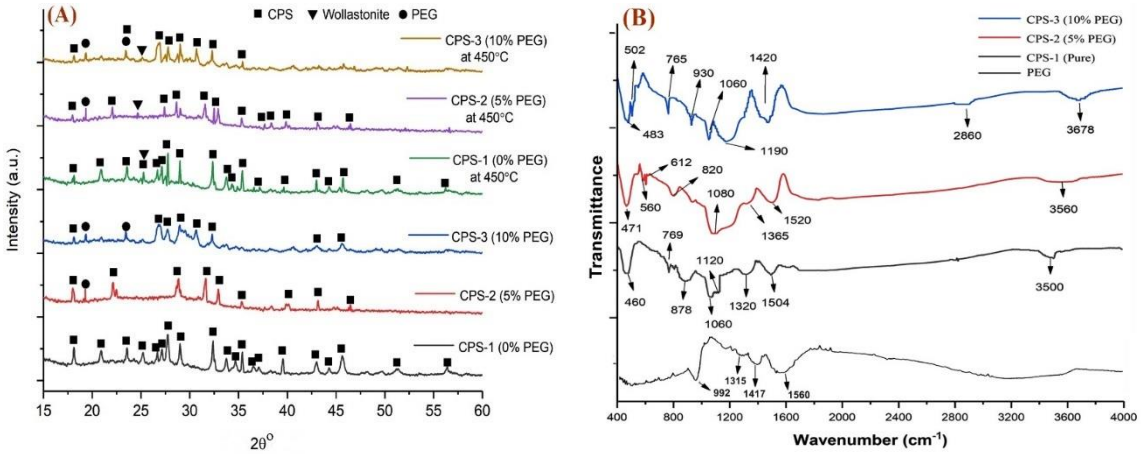

Figure 2. Typical (**A**) XRD pattern and (**B**) FTIR spectra of porous calcium phosphate silicate.

FTIR (Figure 2B) spectrum data revealed O–H stretching vibrations observed at 3500, 3560 and 3678 cm^{-1} [34,35] and O–H deformation at 765 and 769 cm^{-1}. The band occurred at 2860 cm^{-1} due to the existence of the C–H group stretching in CPS-3 as a result of the presence of PEG [36]. The intense bands within 450–510 cm^{-1} correspond to Si–O–, P–O, PO_4^{3-} and SiO_4^{4-}, while the absorption bands at 1060 cm^{-1} assigned to the vibration of the Si–O–Si [30,34]. The functional group SiO_4^{4-} was also recognized by nearly at 612 and 878 cm^{-1} [30]. The absorption bands at 820 and 878 cm^{-1} represent Si–CH_3 and SiO_4^{4-} functional groups. The band between 1000–1200 cm^{-1} is associated with the Si–O– stretching, while the band at 930 cm^{-1} corresponds to Si–O– with one non-bridging oxygen [34]. The appearance of a medium stretching vibration at 1320 cm^{-1} was because of the C=O group. The pure PEG sample showed bands at 992, 1315, 1417 and 1560 cm^{-1} while PEG-modified sample showed bands at 1320 and 1365 cm^{-1}, denoting CH_3 and C–O stretching vibrations.

3.2. Morphologic Characterizations of Calcium Phosphate Silicate Materials

The high-resolution 2 D TEM images revealed the particle size estimation of PEG-modified CPS-1 (Figure 3A,B), CPS-2 (Figure 3C,D) and CPS-3 (Figure 3E,F) samples. Figure 3A shows a 506-nm-sized crystalline particle of CPS-1. CPS-2 (Figure 3C) revealed 265.4-nm-sized irregular particles while CPS-3 has not revealed any proper shape. Crystallite size is calculated using the Scherrer formula from XRD patterns for all synthesized samples. The calculated crystal size of CPS-1, CPS-2 and CPS-3 is 24,

18 and 15 nm, respectively. These calculated results are quite different from TEM results. Because the crystallite size determined using Scherrer formula from XRD patterns provided an average value of the bulk sample since the diffraction occurs from a considerable volume of the sample. Apart from that in TEM, we found the crystallite size from a very local area that may not be the representative size of the bulk sample. Removal of PEG at high temperatures during heat treatment may lead to a highly ordered porous structure, as observed in CPS-2 and CPS-3 (Figure 3). At the 200-nm-scale, all the samples showed significant structural differences; CPS-1 (0% PEG) looked like a dense material, while CPS-3 (10% PEG) displayed a better porous structure than the CPS-2 (5% PEG) sample.

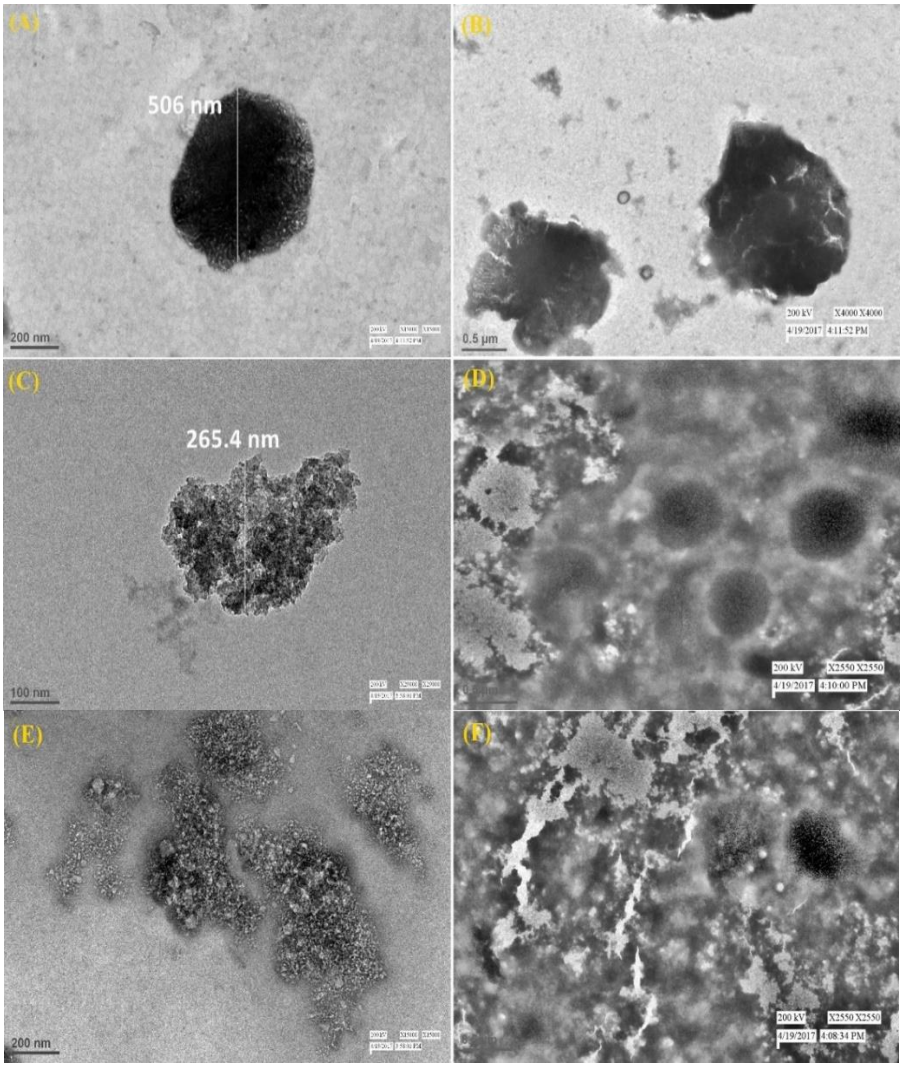

Figure 3. Typical transmission electron microscopy (TEM) analysis of Ca5(PO4)2SiO4 (CPS)-1 (**A**,**B**), CPS-2 (**C**,**D**) and CPS-3 (**E**,**F**).

The increment of PEG concentration (more than 10% *w*/*v*) led to the densification of materials, which reduced the porosity of the CPS. The SEM results revealed the irregular micro size crystalline particles of CPS-1 (Figure 4A) and CPS-2 (Figure 4B) revealed amorphous particles. The SEM image of CPS-3 showed a porous microstructure, observed after the removal of PEG after heat treatment, see Figure 4C. The morphology of this specimen significantly display that will be beneficial for future applications, for instance tissue engineering and drug loading. The optimized favorite sample CPS-3 was used investigated through EDS analysis (Figure 4D) which showed the relative concentration of the Si, Ca, P and C elements in the synthesized sample. The results obtained from EDS analysis depend on several factors, to name a few, sample topography, beam parameters, field noises (electronic and

external fields), acquisition settings, detector type and atomic number of the elements. From particle size distribution histogram (Figure 4E), it is concluded that particle size of CPS-1 is to be under 10 µm, for CPS-2 it is estimated to be under 100 µm, while for CPS-3, it observed to be under 160 µm due to agglomeration of particles.

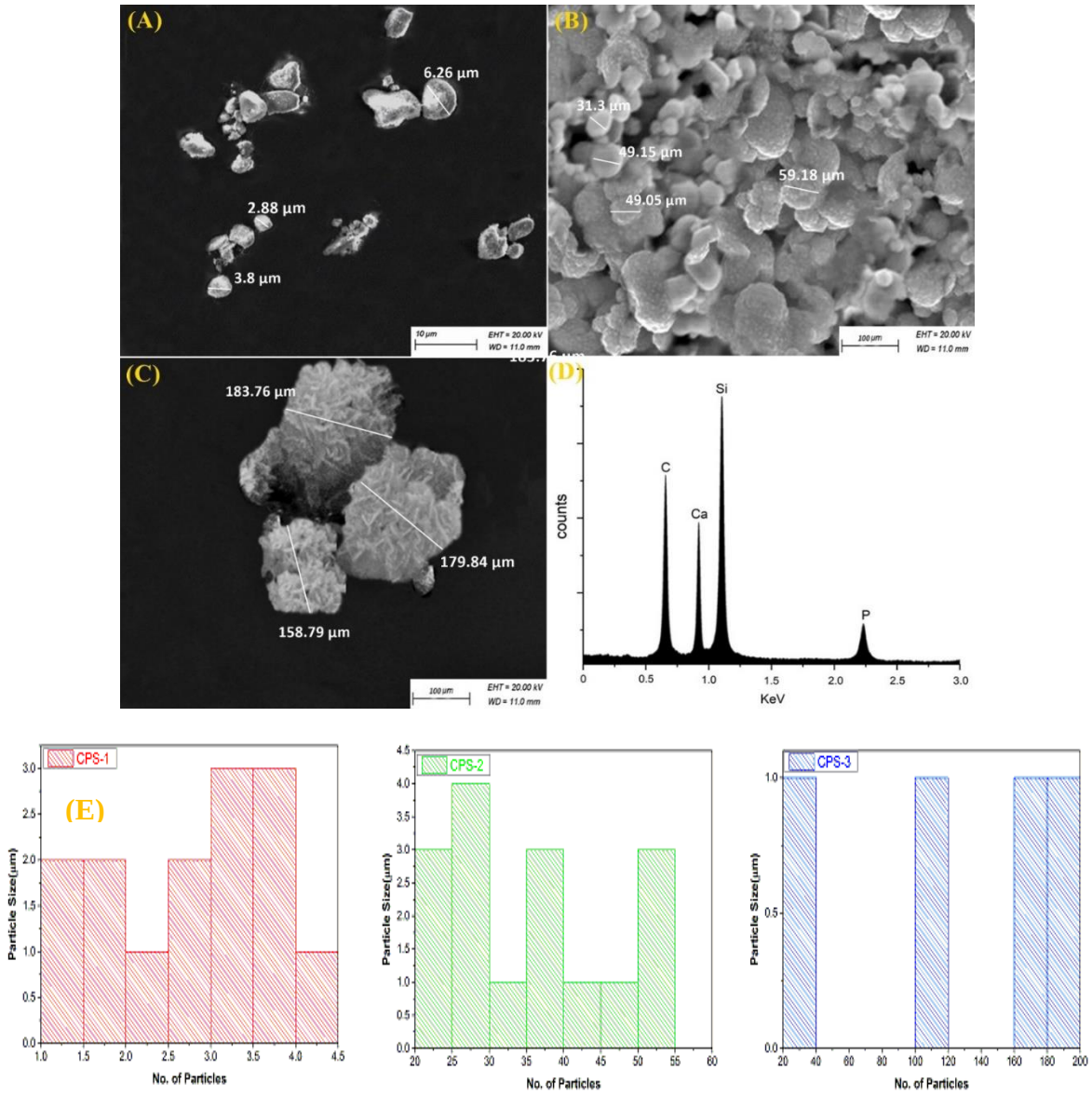

Figure 4. Typical SEM analysis of CPS-1 (**A**), CPS-2 (**B**), CPS-3 (**C**), energy dispersive spectroscopy (EDS) spectrum of CPS-3 (**D**) and particle size distribution histogram for CPS-1, CPS-2, CPS-3 (**E**).

3.3. Porosity Measurements for Calcium Phosphate Silicate Materials

The Brunauer, Emmett and Teller (BET) method is a promising technique to determine the surface area through physical adsorption–desorption isotherm analysis [37]. The porosity of a material depends upon the concentration and type or nature of the template used during the fabrication process [38]. The reparative bone formation and inflammatory response are also influenced by the morphologies of the materials [39,40]. From BET analysis (Figure 5A,B), CPS-3 revealed a surface area of 30.6672 $m^2 \cdot g^{-1}$, pore volume of 0.9722 $cm^3 \cdot g^{-1}$ and pore diameter of 4.58 nm, while CPS-2 revealed a surface area of 27.9840 $m^2 \cdot g^{-1}$, pore volume of 0.6243 $cm^3 \cdot g^{-1}$ and pore diameter of 2.84 nm. The addition of PEG affects the microstructure as well as the porosity of the CPS. The BET result revealed that the

CPS-3 (10% PEG) has shown better porosity that will be a key factor in application part. At 450 °C, the decomposition of PEG generated the porous network. The bio factors include genes or cells, proteins and nutrients can easily exchange through the porous structure of materials. Porosity and pore size possess high impact on the application of the material [3,41].

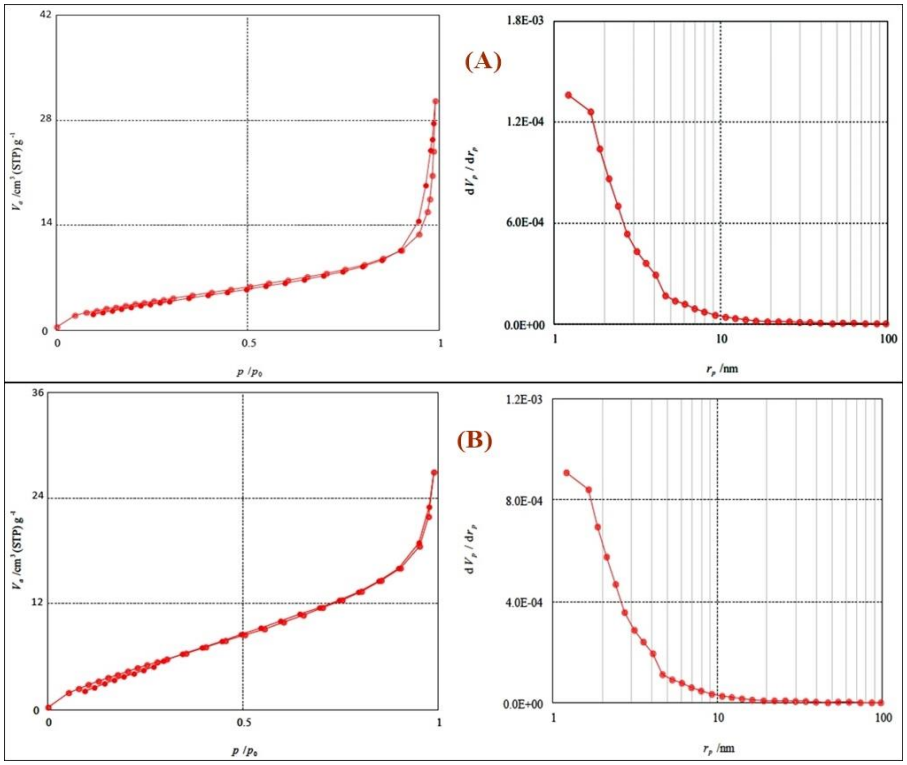

Figure 5. Adsorption–desorption isotherm and Barrett, Joyner, and Halenda (BJH) plot of CPS-3 (**A**) and CPS-2 (**B**).

3.4. Bioactivity Analysis

SBF provides the same environment as blood plasma, where surface dissolution starts mineralization through the slow release of ions in the solvent [33]. When materials were immersed in the SBF solution, a set of reactions such as ion exchange, precipitation and dissolution occurred for the apatite formation [42]. The SBF treatment generated two new groups, CO_3^{2-} and PO_4^{3-}, at 1420 and 1480 cm^{-1}, which are due to the absorbance of CO_2 (Figure 6D). The generation of new compounds are directed by both the immersion parameters (immersion time, temperature and pH, temperature) and surface characteristics of the materials [43]. The presence of CO_3^{2-} and PO_4^{3-} groups are associated with apatite formation on the surface of the sample after a seven-day immersion [30,44]. Further, CO_3^{2-} and PO_4^{3-} ions contribute to nucleation and subsequent surface mineralization that leads to actual apatite formation [45,46]. The in vitro apatite-forming ability of material often successfully predicts the actual bioactivity of biomaterials [47]. The bands at 1653 and 1470 cm^{-1} denoted CO_3^{2-}, while peaks at 1314 and 2790 cm^{-1} were attributed to C–H group. The peaks appearing at 561 and 880 cm^{-1} are due to bending mode of O–P–O and variable symmetry of HPO_4^{3-}, respectively [48]. The band at 1025 cm^{-1} was assigned to the presence of the PO_4^{3-} group [49,50]. The surface of the material released Ca^{2+}, HPO_4^{2-} and PO_4^{3-} ions and absorbed calcium and phosphate ions from SBF. The incorporation of other electrolytes, such as CO_3^{2-} and Mg^{2+} ions, started to generate the apatite layer [51]. The mineralization behavior of CPS-1, CPS-2 and CPS-3 was shown in Figure 6A–C and also confirmed through FTIR results, as shown in Figure 6D.

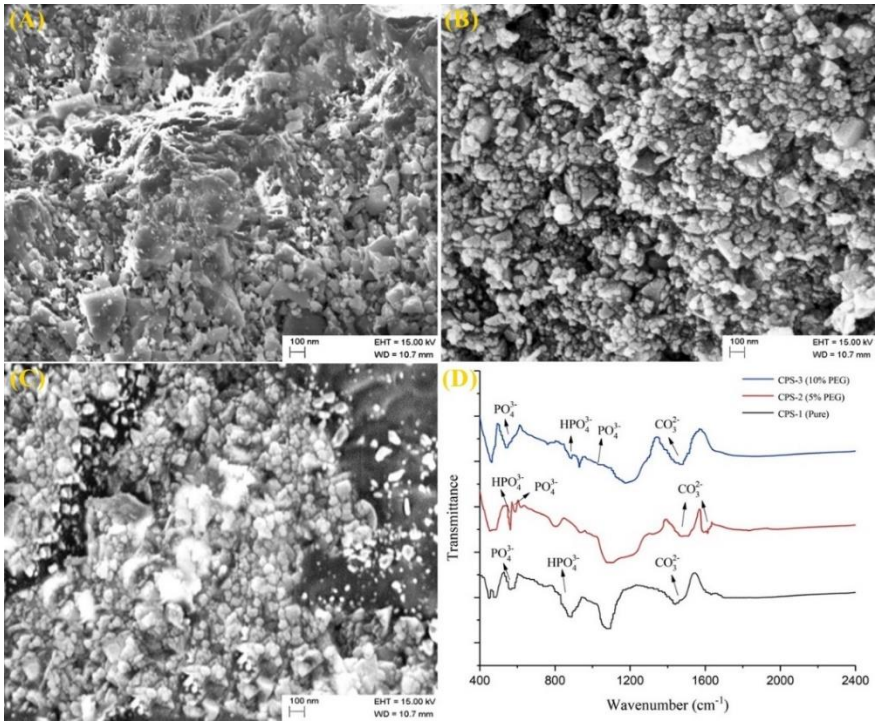

Figure 6. SEM analysis of synthetic body fluid (SBF)-treated CPS-1 (**A**), CPS-2 (**B**), CPS-3 (**C**) and FTIR analysis (**D**).

3.5. Thermal Gravimetric Analysis

The physical and morphologic transformations of the PEG-modified CPS samples analyzed through thermal gravimetric analysis. It is well known that the chemical structures are altered by heat treatment as it leads to the thermal decomposition of the materials. TGA results presented in Figure 7, weight loss in CPS-1 and CPS-2 divided into three main steps (S-1, S-2 and S-3): removal of –OH groups, polymeric phase (PEG) and burnout of the CPS mass (Ca, P and Si) while CPS-3 revealed weight loss in two stages. In all the samples, the initial weight loss was confirmed because of the release of absorbed moisture contents. CPS-2 and CPS-3 showed more weight loss than CPS-1 that was because of the PEG thermal degradation within a temperature range of around 250–300 °C. CPS-3 fabricated with 10% PEG but thermal decomposition of the organic groups, generated porous microstructure and microporous materials showed large specific surface that support more degradation at high temperature.

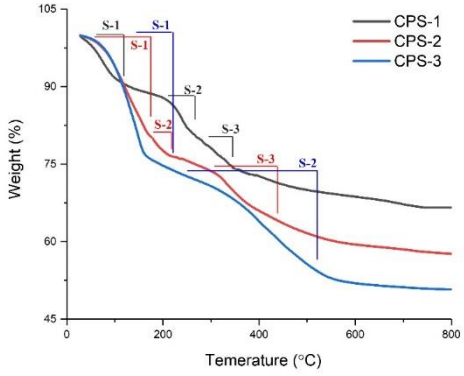

Figure 7. Thermos-gravimetric analysis (TGA) analysis of CPS-1, CPS-2 and CPS-3.

4. Conclusions

In summary, the effect of PEG on various properties of CPS was investigated. The use of PEG improves the morphology, physiology and bioactivity of CPS. Porosity and bioactivity of sol-gel-derived samples were greatly influenced by varying the concentration of PEG. The heat treatment at 450 °C plays an important role in the phase modification and porosity generation. This could be attributed, as the concentration of PEG increased, the densification and agglomeration in particles were observed. The formation of the apatite layer on the surface of SBF treated CPS exposed mineralization. PEG-modified $Ca_5(PO_4)_2SiO_4$ demonstrated better in vitro bioactivity than pure CPS, by tempting bone-like apatite in the artificial salt solution SBF. PEG-modified $Ca_5(PO_4)_2SiO_4$ bioceramic (CPS-3) is different from those in conventional material and may be a promising material for implant coatings, drug loading and bone regeneration applications. Future works should determine the optimum concentration for controlled porosity and their applications in soft as well as hard tissue engineering.

Author Contributions: Conception and design of the experiments, P.K., M.S., V.K., B.S.D., A.S., H.F., N.A., A.M. and M.H. implementation of the experiments, analysis of the data, the contribution of the analysis tools and writing the study. All authors have read and agreed to the published version of the manuscript.

Funding: The authors would like to extend their sincere appreciation to the Deanship of Scientific Research at King Saud University for funding this research group (No. RGP-1435-052).

Acknowledgments: The authors would like to extend their sincere appreciation to the Deanship of Scientific Research at King Saud University, Kingdom of Saudi Arabia for support.

Conflicts of Interest: The authors declare no conflict of interest.

References

1. Wu, C.; Chang, J. A review of bioactive silicate ceramics. *Biomed. Mater.* **2013**, *8*, 32001. [CrossRef]
2. Duan, W.; Ning, C.; Tang, T. Cytocompatibility and osteogenic activity of a novel calcium phosphate silicate bioceramic: Silicocarnotite. *J. Biomed. Mater. Res. Part A* **2013**, *101A*, 1955–1961. [CrossRef] [PubMed]
3. Bordbar-Khiabani, A.; Yarmand, B.; Mozafari, M. Emerging magnesium-based biomaterials for orthopedic implantation. *Emerg. Mater. Res.* **2019**, *8*, 305–319. [CrossRef]
4. Lu, W.; Duan, W.; Guo, Y.; Ning, C. Mechanical properties and in vitro bioactivity of $Ca_5(PO_4)_2SiO_4$ bioceramic. *J. Biomater. Appl.* **2012**, *26*, 637–650. [CrossRef] [PubMed]
5. Kumar, P.; Dehiya, B.S.; Sindhu, A. Comparative study of chitosan and chitosan-gelatin scaffold for tissue engineering. *Int. Nano Lett.* **2017**, *7*, 285–290. [CrossRef]
6. Ji, D.D.; Xu, J.Y.; Gu, X.F.; Zhao, Q.M.; Gao, A.G. Preparation, characterization and biocompatibility of bioactive coating on titanium by plasma electrolytic oxidation. *Sci. Adv. Mater.* **2019**, *11*, 1411–1415. [CrossRef]
7. Wang, P.; He, H.; Cai, R.; Tao, G.; Yang, M.; Zuo, H.; Umar, A.; Wang, Y. Cross-linking of dialdehyde carboxymethyl cellulose with silk sericin to reinforce sericin film for potential biomedical application. *Carbohydr. Polym.* **2019**, *212*, 403–411. [CrossRef]
8. Li, J.; Wu, L.; Shen, R.; Hou, Y.; Chen, Z.; Cai, M.; Wei, Z.; Chen, X.; Gao, J. Preparation and biocompatibility of corrosion resistant micro-nano dual structures on the surface of TAx pure titanium dental implants. *Sci. Adv. Mater.* **2019**, *11*, 1656–1665. [CrossRef]
9. Kumar, P.; Dehiya, B.S.; Sindhu, A. Bioceramics for hard tissue engineering applications: A review. *Int. J. Appl. Eng. Res.* **2018**, *13*, 2744–2752.
10. Deng, F.; Wang, F.; Liu, Z.; Kou, H.; Cheng, G.; Ning, C. Enhanced mechanical property of $Ca_5(PO_4)_2SiO_4$ bioceramic by a biocompatible sintering aid of zinc oxide. *Ceram. Int.* **2018**, *44*, 18352–18362. [CrossRef]
11. Chaudhary, S.; Umar, A.; Mehta, S. Surface functionalized selenium nanoparticles for biomedical applications. *J. Biomed. Nanotechnol.* **2014**, *10*, 3004–3042. [CrossRef] [PubMed]
12. Shad, A.A.; Ahmad, S.; Ullah, R.; AbdEl-Salam, N.M.; Fouad, H.; Rehman, N.U.; Hussain, H.; Saeed, E. Phytochemical and biological activities of four wild medicinal plants. *Sci. World J.* **2014**, 857363. [CrossRef] [PubMed]

13. Kumar, P. Nano-TiO_2 doped chitosan scaffold for the bone tissue engineering applications. *Int. J. Biomater.* **2018**, 6576157. [CrossRef]
14. Elliott, J.E.; Macdonald, M.; Nie, J.; Bowman, C.N. Structure and swelling of poly(acrylic acid) hydrogels: Effect of pH, ionic strength, and dilution on the crosslinked polymer structure. *Polymer (Guildf.)* **2004**, *45*, 1503–1510. [CrossRef]
15. Jones, D.S.; Andrews, G.P.; Gorman, S.P. Characterization of crosslinking effects on the physicochemical and drug diffusional properties of cationic hydrogels designed as bioactive urological biomaterials. *J. Pharm. Pharmacol.* **2005**, *57*, 1251–1259. [CrossRef]
16. Sun, Q.; Yuan, Y.; Zhang, H.; Cao, X.; Sun, L. Thermal properties of polyethylene glycol/carbon microsphere composite as a novel phase change material. *J. Therm. Anal. Calorim.* **2017**, *130*, 1741–1749. [CrossRef]
17. Paul, W.; Sharma, C.P. Polyethylene glycol modified calcium phosphate microspheres facilitate selective adsorption of immunogobulin G from human blood. *Trends Biomater. Artif. Organs* **2013**, *27*, 20–28.
18. Nagar, P.; Goyal, P.; Gupta, A.; Sharma, A.K.; Kumar, P. Synthesis, characterization and evaluation of retinoic acid-polyethylene glycol nanoassembly as efficient drug delivery system. *Nano Struct. Nano Objects* **2018**, *14*, 110–117. [CrossRef]
19. Mohaisen, M.; Yildirim, R.; Yilmaz, M.; Durak, M. Production of functional yogurt drink, apple and orange juice using nano-encapsulated l. brevis within sodium alginate-based biopolymers. *Sci. Adv. Mater.* **2019**, *11*, 1788–1797. [CrossRef]
20. Dave, V.; Gupta, A.; Singh, P.; Gupta, C.; Sadhu, V.; Reddy, K.R. Synthesis and characterization of celecoxib loaded PEGylated liposome nanoparticles for biomedical applications. *Nano Struct. Nano Objects* **2019**, *18*, 100288.
21. Zhang, X.; Zeng, D.; Li, N.; Wen, J.; Jiang, X.; Liu, C.; Li, Y. Functionalized mesoporous bioactive glass scaffolds for enhanced bone tissue regeneration. *Sci. Rep.* **2016**, *6*, 19361. [CrossRef] [PubMed]
22. Kumar, P.; Dehiya, B.S.; Sindhu, A. Synthesis and characterization of nHA-PEG and nBG-PEG scaffolds for hard tissue engineering applications. *Ceram. Int.* **2019**, *45*, 8370–8379. [CrossRef]
23. Ansari, S.G.; Fouad, H.; Shin, H.S.; Ansari, Z.A. Electrochemical enzyme-less urea sensor based on nano tim oxide synthesized by hydrothermal technique. *Chem. Biol. Interact.* **2015**, *242*, 45–49. [CrossRef] [PubMed]
24. Algarni, H.; AlShahrani, I.; Ibrahim, E.H.; Eid, R.A.; Kilany, M.; Ghramh, H.A.; Abdellahi, M.O.; Sayed, M.A.; Yousef, E.S. In-vitro bioactivity of optical glasses containing strontium oxide (SrO). *J. Nanoelectron. Optoelectron.* **2019**, *14*, 1105–1112. [CrossRef]
25. Ansari, F.; Soofivand, F.; Salavati-Niasari, M. Eco-friendly synthesis of cobalt hexaferrite and improvement of photocatalytic activity by preparation of carbonic-based nanocomposites for waste-water treatment. *Compos. Part B Eng.* **2019**, *165*, 500–509. [CrossRef]
26. Ansari, F.; Sobhani, A.; Salavati-Niasari, M. Simple sol-gel synthesis and characterization of new $CoTiO_3$/$CoFe_2O_4$ nanocomposite by using liquid glucose, maltose and starch as fuel, capping and reducing agents. *J. Colloid Interface Sci.* **2018**, *514*, 723–732. [CrossRef]
27. Owens, G.J.; Singh, R.K.; Foroutan, F.; Alqaysi, M.; Han, C.-M.; Mahapatra, C.; Kim, H.-W.; Knowles, J.C. Sol-gel based materials for biomedical applications. *Prog. Mater. Sci.* **2016**, *77*, 1–79. [CrossRef]
28. Algarni, H.; Alshahrani, I.; Ibrahim, E.; Eid, R.; Kilany, M.; Ghramh, H.; Sayed, M.; Reben, M.; Yousef, E. Structural, thermal stability and in vivo bioactivity properties of nanobioglasses containing ZnO. *Sci. Adv. Mater.* **2019**, *11*, 925–935. [CrossRef]
29. Rao, S.H.; Harini, B.; Shadamarshan, R.P.K.; Balagangadharan, K.; Selvamurugan, N. Natural and synthetic polymers/bioceramics/bioactive compounds-mediated cell signalling in bone tissue engineering. *Int. J. Biol. Macromol.* **2018**, *110*, 88–96. [CrossRef]
30. Radev, L.; Hristov, V.; Michailova, I.; Samuneva, B. Sol-gel bioactive glass-ceramics Part I: Calcium phosphate silicate/ wollastonite glass-ceramics. *Cent. Eur. J. Chem.* **2009**, *7*, 317–321. [CrossRef]
31. Lombardi, M.; Gremillard, L.; Chevalier, J.; Lefebvre, L.; Cacciotti, I.; Bianco, A.; Montanaro, L. A comparative study between melt-derived and sol-gel synthesized 45S5 bioactive glasses. *Key Eng. Mater.* **2013**, *541*, 15–30. [CrossRef]
32. Matsuda, A.; Matsuno, Y.; Katayama, S.; Tsuno, T.; Tohge, N.; Minami, T. Physical and chemical properties of titania-silica films derived from poly(ethylene glycol)-containing gels. *J. Am. Ceram. Soc.* **1990**, *73*, 2217–2221. [CrossRef]

33. Kumar, P.; Dehiya, B.S.; Sindhu, A. Ibuprofen-loaded CTS/nHA/nBG scaffolds for the applications of hard tissue engineering. *Iran. Biomed. J.* **2019**, *23*, 190–199. [CrossRef] [PubMed]
34. Ouis, M.; Abdelghany, A.; Elbatal, H. Corrosion mechanism and bioactivity of borate glasses analogue to Hench's bioglass. *Process. Appl. Ceram.* **2012**, *6*, 141–149. [CrossRef]
35. Davar, F.; Salavati-Niasari, M.; Mir, N.; Saberyan, K.; Monemzadeh, M.; Ahmadi, E. Thermal decomposition route for synthesis of Mn_3O_4 nanoparticles in presence of a novel precursor. *Polyhedron* **2010**, *29*, 1747–1753. [CrossRef]
36. Kumar, P.; Saini, M.; Dehiya, B.S.; Umar, A.; Sindhu, A.; Mohammed, H.; Al-Hadeethi, Y.; Guo, Z. Fabrication and in-vitro biocompatibility of freeze-dried CTS-nHA and CTS-nBG scaffolds for bone regeneration applications. *Int. J. Biol. Macromol.* **2020**, *149*, 1–10. [CrossRef]
37. Salavati-Niasari, M. Ship-in-a-bottle synthesis, characterization and catalytic oxidation of styrene by host (nanopores of zeolite-Y)/guest ([bis(2-hydroxyanil)acetylacetonato manganese(III)]) nanocomposite materials (HGNM). *Microporous Mesoporous Mater.* **2006**, *95*, 248–256. [CrossRef]
38. Kumar, P.; Saini, M.; Kumar, V.; Singh, M.; Dehiya, B.S.; Umar, A.; Ajmal Khan, M.; Alhuwaymel, T.F. Removal of Cr (VI) from aqueous solution using VO2(B) nanoparticles. *Chem. Phys. Lett.* **2019**, 136934. [CrossRef]
39. Sampath, U.G.T.M.; Ching, Y.C.; Chuah, C.H.; Sabariah, J.J.; Lin, P.-C. Fabrication of porous materials from natural/synthetic biopolymers and their composites. *Materials* **2016**, *9*, 991. [CrossRef]
40. Fathi, M.H.; Hanifi, A.; Mortazavi, V. Preparation and bioactivity evaluation of bone-like hydroxyapatite nanopowder. *J. Mater. Process. Technol.* **2008**, *202*, 536–542. [CrossRef]
41. Jiang, Y.; Lawrence, M.; Ansell, M.P.; Hussain, A. Cell wall microstructure, pore size distribution and absolute density of hemp shiv. *R. Soc. Open Sci.* **2018**, *5*, 171945. [CrossRef] [PubMed]
42. Stanciu, G.A.; Sandulescu, I.; Savu, B.; Stanciu, S.G.; Paraskevopoulos, K.M.; Chatzistavrou, X.; Kontonasaki, E.; Koidis, P. Investigation of the hydroxyapatite growth on bioactive glass surface. *J. Biomed. Pharm. Eng.* **2007**, *1*, 34–39.
43. Shin, K.; Acri, T.; Geary, S.; Salem, A.K. Biomimetic mineralization of biomaterials using simulated body fluids for bone tissue engineering and regenerative medicine. *Tissue Eng. Part A* **2017**, *23*, 1169–1180. [CrossRef] [PubMed]
44. Radev, L.; Hristov, V.; Michailova, I.; Fernandes, H.M.V.; Salvado, M.I.M. In vitro bioactivity of biphasic calcium phosphate silicate glass-ceramic in CaO-SiO_2-P_2O_5 system. *Process. Appl. Ceram.* **2010**, *4*, 15–24. [CrossRef]
45. Algarni, H.; Shahrani, I.; Ibrahim, E.; Eid, R.; Kilany, M.; Ghramh, H.; Ali, A.; Yousef, E. Silver Modified tricalcium phosphate for biomedical application: Structural investigation and study of antimicrobial with histopathological activity. *Sci. Adv. Mater.* **2019**, *11*, 1383–1391. [CrossRef]
46. Zadpoor, A.A. Relationship between in vitro apatite-forming ability measured using simulated body fluid and in vivo bioactivity of biomaterials. *Mater. Sci. Eng. C* **2014**, *35*, 134–143. [CrossRef]
47. Meejoo, S.; Maneeprakorn, W.; Winotai, P. Phase and thermal stability of nanocrystalline hydroxyapatite prepared via microwave heating. *Thermochim. Acta* **2006**, *447*, 115–120. [CrossRef]
48. Destainville, A.; Champion, E.; Bernache-Assollant, D.; Laborde, E. Synthesis, characterization and thermal behavior of apatitic tricalcium phosphate. *Mater. Chem. Phys.* **2003**, *80*, 269–277. [CrossRef]
49. Algarni, H.; Alshahrani, I.; Ibrahim, E.; Eid, R.; Kilany, M.; Ghramh, H.; Ali, A.; Yousef, E. Fabrication and biocompatible characterizations of bio-glasses containing oxyhalides ions. *J. Nanoelectron. Optoelectron.* **2019**, *14*, 328–334. [CrossRef]
50. Clupper, D.C.; Hench, L.L. Bioactive response of Ag-doped tape cast Bioglass®45S5 following heat treatment. *J. Mater. Sci. Mater. Med.* **2001**, *12*, 917–921. [CrossRef]
51. Algarni, H.; AlShahrani, I.; Ibrahim, E.; Eid, R.; Kilany, M.; Ghramh, H.; Abdellahi, M.; Shaaban, E.; Reben, M.; Yousef, E. Synthesis, Mechanical, In Vitro and In vivo bioactivity and preliminary biocompatibility studies of bioglasses. *Sci. Adv. Mater.* **2019**, *11*, 1458–1466. [CrossRef]